Study of nonlinear spectral energy transfer in frequency domain

M. Xu, G. R. Tynan, C. Holland, Z. Yan, S. H. Muller, and J. H. Yu
Center for Energy Research, University of California, San Diego, La Jolla, California 92093, USA

(Received 9 December 2008; accepted 30 January 2009; published online 23 April 2009)

A method for measuring nonlinear energy transfer in the frequency domain using a two-field model of drift turbulence is proposed, and the theoretical motivation and experimental results are presented. The approach is based on the cross-bispectral analysis of quadratic nonlinearities in the turbulent internal and kinetic energy balance equations directly derived from the fluid plasma continuity and momentum equations. Application of the technique to data from a laboratory plasma experiment reveals the nonlinear energy transfer in weak collisional plasma drift turbulence; the results show a transfer of density fluctuation energy toward higher frequency (which correspond to smaller azimuthal spatial scales) and a transfer of kinetic energy to lower frequencies (corresponding to larger azimuthal scales). © *2009 American Institute of Physics*.
[DOI: 10.1063/1.3098538]

I. INTRODUCTION

The study of nonlinear dynamics of drift-wave turbulence, and specifically the study of how large spatial scale fluctuations and zonal flows are generated by nonlinear processes and of how the resulting shear flows affect the turbulent density fluctuation scale lengths directly addresses the underlying physics for zonal/shear flow generation,[1,2] gyro-Bohm/Bohm scaling,[3] and the origins of critical gradient transport scaling in magnetically confined plasmas,[4] as well as provides tests of fundamental turbulence theory. As a result, the nonlinear spectral energy transfer mediated via wave-wave coupling has received significant attention, as given in Refs. 1 and 5–10. The bispectrum, which is related to the degree of phase correlation among three waves, was introduced to the plasma physics community by Kim and Powers[11] to study the quadratic nonlinearity of plasma fluctuations, and was motivated by earlier applications of this technique to neutral fluid turbulence, see, for example, Refs. 12–14. By assuming the detailed form of three-wave coupling and deriving a power balance equation, Kim *et al.*[10] went further and developed a way to experimentally determine the coupled energy flow among different spectral components. In that work, the wave coupling coefficient had to be known *a priori* in order to know this power transfer due to the three-wave coupling.

Using a single-field model suitable for turbulence with very small parallel electron dissipation, Ritz *et al.*[15] then developed and subsequently Kim *et al.*[16] refined a method which enables one to quantitatively estimate the growth rate γ_k, dispersion relation $\bar{\omega}_k$, and the wave-wave coupling coefficient $\Lambda_k^Q(k_1,k_2)$, from which the power transferred through nonlinear coupling can be calculated from experimental data. In order to obtain two coupled equations that yield the growth rate, dispersion relation and coupling coefficient, the fourth-order spectral moment that occurs in their work was approximated by the square of the second-order moment using the Millionshchikov approximation.[17] This method was derived in the wavenumber domain and in principle requires a knowledge of the temporal behavior of the Fourier transformed potential $\phi(k,t)$ (which is obtained from simultaneous multipoint turbulence measurements) to perform the calculation. As a result, a simultaneous measurement at a large number of spatially localized points is typically required, which is challenging due to practical (i.e., large number of channels) and physical (i.e., measuring turbulence properties without much disturbance) limitations. These works then used the Taylor frozen flow hypothesis to relate wavenumber to frequency, and then argued that the energy transfer could then be studied in the frequency domain, thereby avoiding the requirement for a large number of spatial measurements.

Another concern in applying these techniques arises from the multifield nature of plasma turbulence. Turbulence in magnetic fusion plasmas is characterized by fluctuations in density, potential, temperature, and magnetic field, and these fluctuations can influence the turbulence dynamics and resulting transport. All the methods mentioned above assume that the observation of one field is sufficient to describe the nonlinearity in the plasma, and the effects introduced by cross-field interaction are small. For example, turbulence in magnetic fusion confinement devices clearly exhibits multifield dynamics as shown, e.g., by the fact that the normalized amplitudes of density and potential fluctuations are not equal,[18] in clear violation of the underlying assumptions of all single-field drift turbulence models. Furthermore in the edge plasma region where these techniques are usually applied there is a large phase shift between the density and potential fluctuations,[18] again invalidating the fundamental model on which these single-field energy transfer models are based. In low temperature plasmas found e.g., in the controlled shear decorrelation experiment (CSDX) (UC San Diego) device[19] used in this work, the measured density and potential fields have a cross correlation significantly less than unity, as shown by Fig. 3(d), and have a nonzero density-potential cross phase, again in clear violation of the assumptions of single-field models. Similar observations hold for the turbulence in the edge and scrape-off layer region of confinement experiments. As a result, studies of turbulence nonlin-

ear dynamics that are to be compared against such experiments should include at least two fields (e.g., at least density and velocity or electrostatic potential as well as temperature fluctuations if those are important for the turbulence dynamics) and cannot rely upon models that are based upon the single-field model of drift turbulence.

Nonlinear energy transfer in simple models of drift-wave turbulence has been extensively studied by many groups using both analytic and computational approaches (see, for instance, the work by Camargo *et al.*[20] for a comprehensive numerical investigation of the issue). Recently Manz *et al.*[21] analyzed experimental measurements in wavenumber space using a single-field model applied separately to density and potential measurements and showed that turbulent density fluctuation energy was transferred to small scales, while turbulent kinetic energy was transferred to large scales. The first use of a multifield approach to study nonlinear turbulence dynamics via direct calculation of cross bispectra was performed by Holland *et al.*[22] using beam emission spectroscopy (BES) data. The results showed that radially sheared, oscillating poloidal velocity of a geodesic acoustic mode caused the density fluctuation energy to move toward higher frequency. A brief discussion of multifield nonlinear energy transfer in drift turbulence was also included in the most recent paper by Tynan *et al.*[23]

In this paper we propose a technique to study the nonlinear transfer of turbulence energy in the frequency domain in a system that is described by two fields (density and potential). By combining the derived energy balance equations with a cross-bispectral analysis of the nonlinear terms, the nonlinear energy transfer due to the wave-wave interactions of the drift fluctuations can be determined. Although it is not discussed here, the technique can also be extended in a straightforward manner to turbulence involving temperature fluctuations.

The rest of this paper is arranged as follows: Sec. II presents the theoretical derivation and interpretation of nonlinear energy transfer coefficients and their realization in experiments. Section III gives a brief description about the experimental setup. Section IV is a sample of experimental results of nonlinear energy transfer. Section V includes a summary of the contents and some discussions.

II. THEORETICAL DERIVATION AND INTERPRETATION OF NONLINEAR ENERGY TRANSFER TERMS

Although a similar derivation of spectral energy transfer terms was reported, as given in Ref. 20, and in particular the derivation and study of internal energy transfer in frequency space has been published in Ref. 22, a brief derivation for both internal and kinetic energy transfer terms in frequency domain is included here to help to understand the experimental results from both technical and physical perspective of views. The three-wave coupling enters when a Fourier transform is performed on either the continuity or momentum equation, with the convective derivative $\underline{u}\cdot\nabla n$ or $\underline{u}\cdot\nabla\underline{u}$, where $\underline{u}$ is the fluid velocity that is approximated by $\underline{u}\approx-(\nabla_\perp\phi\times\underline{B}/B^2)$ in the following derivation. From electron momentum and electron continuity equations, an energy transport equation for the spectra of density fluctuations is derived in the frequency domain.

The electron continuity equation:

$$\frac{\partial n_e}{\partial t}+\nabla_\perp\cdot(n_e\underline{u}_{e\perp})+\frac{\partial}{\partial z}(n_e u_{e\|})=0 \tag{1}$$

in which the electron velocity perpendicular to magnetic field is dominated by $\underline{E}\times\underline{B}$ and diamagnetic drift, can be written as (with the unit vector in the magnetic field direction denoted by $\hat{z}$ and quasineutral assumption $n_e\approx n_i=n$ applied)

$$\left(\frac{\partial}{\partial t}+\underline{u}_\perp\cdot\nabla_\perp\right)n=-\frac{\partial}{\partial z}(nu_\|), \tag{2}$$

where $\underline{u}_\perp=\hat{z}\times\nabla_\perp\phi/B$ is the $\underline{E}\times\underline{B}$ velocity. The plasma density fluctuations can be represented in the frequency domain by $n(\underline{x},t)=\Sigma_\omega n_\omega(\underline{x},t)e^{i\omega t}$, where we have allowed the coefficients to possibly vary in time (we discuss this point at length below). A similar expression can be used to decompose the velocity into the frequency domain. Therefore we can then write the time derivative in Eq. (2) as

$$\begin{aligned}\frac{\partial n(\underline{x},t)}{\partial t}&=\frac{\partial}{\partial t}\sum_\omega n_\omega(\underline{x},t)e^{i\omega t}\\&=\sum_\omega\left[e^{i\omega t}\frac{\partial n_\omega(\underline{x},t)}{\partial t}+i\omega e^{i\omega t}n_\omega(\underline{x},t)\right]\\&=\sum_\omega\left[\left(\frac{\partial}{\partial t}+i\omega\right)n_\omega(\underline{x},t)\right]e^{i\omega t}.\end{aligned} \tag{3}$$

As we discuss below, there are limitations on the rate of change in the frequency components, which must be tested empirically from experimental data. Next, we Fourier transform Eq. (2) into the frequency domain, and denoting $n_\omega(\underline{x},t)$ as n_ω we then have

$$\frac{\partial}{\partial t}n_\omega+i\omega n_\omega+\sum_{\omega_1}(\underline{u}_{\perp\omega-\omega_1}\cdot\nabla_\perp)n_{\omega_1}=-\frac{\partial}{\partial z}F(nu_\|), \tag{4}$$

where F denotes the Fourier transform. Multiply both sides by the conjugate of n_ω, i.e., n_ω^*,

$$\begin{aligned}&n_\omega^*\frac{\partial n_\omega}{\partial t}+i\omega|n_\omega|^2+\sum_{\omega_1}n_\omega^*(\underline{u}_{\perp\omega-\omega_1}\cdot\nabla_\perp)n_{\omega_1}\\&\quad=-n_\omega^*\frac{\partial}{\partial z}F(nu_\|).\end{aligned} \tag{5}$$

Adding the above equation to its conjugate and ensemble averaging over a sufficient number of realizations, we can form an ensemble-averaged energy conservation equation in the frequency domain:

$$\begin{aligned}\Rightarrow\quad\left\langle\frac{1}{2}\frac{\partial|n_\omega|^2}{\partial t}\right\rangle&=\left\langle-\mathrm{Re}\left[\sum_{\omega_1}n_\omega^*(\underline{u}_{\perp\omega-\omega_1}\cdot\nabla_\perp)n_{\omega_1}\right]\right\rangle\\&\quad+\left\langle-\mathrm{Re}\left[n_\omega^*\frac{\partial}{\partial z}F(nu_\|)\right]\right\rangle.\end{aligned} \tag{6}$$

The above Eq. (6) simply states that the rate of change in internal energy at the frequency ω is determined by quadratic coupling, linear growth or damping at ω, and parallel dissi-

pation of parallel electron motion. The physical meaning of each term is given below:

$$\left\langle \frac{1}{2}\frac{\partial |n_\omega|^2}{\partial t} \right\rangle$$

is the rate of change in density fluctuation spectra n_ω^2 (denoted as the internal energy) at one specific spatial position;

$$\left\langle -\mathrm{Re}\left[\sum_{\omega_1} n_\omega^* (\underline{u}_{\perp \omega-\omega_1} \cdot \nabla_\perp) n_{\omega_1} \right] \right\rangle$$

is the nonlinear wave-wave coupling term that determines how much energy flows into or out of the Fourier component at the frequency of ω due to three-wave coupling. This quadratic nonlinear term comes from the Fourier transform of the convective derivative, which is in the form of a convolution, and thus imposes a selection rule $\omega=\omega_1+\omega_2$ on the nonlinear coupling. Since this nonlinear coupling term is related to density autospectrum, it is called the internal energy transfer term, denoted as T_n here.

Assuming an isothermal plasma, $u_\parallel$ can be obtained from the parallel component of the electron momentum equation. Substituting this result into Eq. (6), then use the following normalizations: $\hat{n}_e \equiv \tilde{n}_e/n_{e0}$, $\hat{\phi} \equiv e\phi/k_B T_e$, $\hat{t} \equiv t/(1/\Omega_{ci})$, $\hat{\nabla}_\perp \equiv \rho_s \nabla_\perp$, $(\partial/\partial z)=(1/\lambda_{\mathrm{efree}})(\partial/\partial \hat{z})$, and $\hat{L}_{nr} \equiv L_{nr}/\rho_s$, where $\rho_s \equiv c_s/\Omega_{ci}=\sqrt{k_B T_e/M\Omega_{ci}^2}$ is the effective ion Larmor radius calculated with electron temperature, $\lambda_{\mathrm{efree}}=u_{\mathrm{the}}/\nu_{ei}=(k_B T_e/m_e)^{1/2}(m_e/n_e e^2 \eta)$ is the electron mean free path, and $L_{nr} \equiv n_0(x)/\nabla_r n_0$ is the local density gradient scale length. By using the quasineutrality assumption and dropping "^", the internal energy equation becomes

$$\left\langle \frac{1}{2}\frac{\partial |n_\omega|^2}{\partial t} \right\rangle = \left\langle -\mathrm{Re}\left[\sum_{\omega_1} n_\omega^* (\hat{z}\times\nabla_\perp \phi_{\omega-\omega_1} \cdot \nabla_\perp) n_{\omega_1} \right] \right\rangle - \left\langle \frac{1}{L_{nr}} \mathrm{Re}[n_\omega^* \nabla_\theta \phi_\omega] \right\rangle + \left\langle \frac{\nu_{ei}}{\Omega_{ci}} \mathrm{Re}\left[n_\omega^* \frac{\partial^2}{\partial z^2}(n_\omega - \phi_\omega) \right] \right\rangle. \tag{7}$$

Here $-\langle (1/L_{nr})\mathrm{Re}[n_\omega^* \nabla_\theta \phi_\omega] \rangle$ indicates that energy can be extracted from the mean density gradient and hence is the linear driving term, and $\langle (\nu_{ei}/\Omega_{ci})\mathrm{Re}[n_\omega^*(\partial^2/\partial z^2)(n_\omega-\phi_\omega)] \rangle$ means that energy can be dissipated via electron-ion collision, hence is the parallel dissipation term. The above Eq. (7) forms the basis of one of the coupled Hasegawa–Wakatani[24] equations; however here it is expressed solely in the frequency domain without the corresponding spatial Fourier transform used in that original work.

By performing a similar process on the ion momentum equation, with the same normalizations as before, an energy balance equation related to velocity fluctuation can be obtained,

$$\left\langle \frac{1}{2}\frac{\partial |\nabla_\perp \phi_\omega|^2}{\partial t} \right\rangle = \left\langle -\mathrm{Re}\sum_{\omega_1} (\hat{z}\times\nabla_\perp \phi_\omega^*) \cdot [(\hat{z}\times\nabla_\perp \phi_{\omega-\omega_1} \cdot \nabla_\perp)(\hat{z}\times\nabla_\perp \phi_{\omega_1})] \right\rangle + \left\langle \frac{\mu_\perp}{\Omega_{ci}\rho_s^2} \mathrm{Re}[(\hat{z}\times\nabla_\perp \hat{\phi}_\omega^*)\cdot\nabla_\perp^2 (\hat{z}\times\nabla_\perp \hat{\phi}_\omega)] \right\rangle + \left\langle -\frac{\nu_{i-n}}{\Omega_{ci}} |\nabla_\perp \phi_\omega|^2 \right\rangle, \tag{8}$$

where $\mu_\perp$ is the ion viscosity, ν_{i-n} is the ion-neutral collision rate, and neutrals have been assumed to have negligible velocity.

The above energy balance equation involves only the plasma potential, in which

$$\left\langle \frac{1}{2}\frac{\partial |\nabla_\perp \phi_\omega|^2}{\partial t} \right\rangle$$

is the rate of change in the $\underline{E}\times\underline{B}$ velocity fluctuation energy at one specific spatial position.

$$\left\langle -\mathrm{Re}\sum_{\omega_1} (\hat{z}\times\nabla_\perp \phi_\omega^*) \cdot [(\hat{z}\times\nabla_\perp \phi_{\omega-\omega_1} \cdot \nabla_\perp)(\hat{z}\times\nabla_\perp \phi_{\omega_1})] \right\rangle$$

determines how much energy is nonlinearly coupled into or out of the frequency ω. Again, a selection rule $\omega=\omega_1+\omega_2$ is imposed on the nonlinear coupling. This nonlinear term is called the kinetic energy transfer term, T_u, due to the fact that it is related to the perpendicular kinetic energy evolution.

$$\left\langle \frac{\mu_\perp}{\Omega_{ci}\rho_s^2} \mathrm{Re}[(\hat{z}\times\nabla_\perp \hat{\phi}_\omega^*)\cdot\nabla_\perp^2 (\hat{z}\times\nabla_\perp \hat{\phi}_\omega)] \right\rangle$$

shows the rate at which energy can be damped due to ion viscosity.

$$\left\langle -\frac{\nu_{i-n}}{\Omega_{ci}} |\nabla_\perp \phi_\omega|^2 \right\rangle$$

is a flow damping term due to ion-neutral collisions, or due to any other damping mechanism (e.g., trapped-passing ion collisions in a torus), that is simply proportional to the turbulent kinetic energy and a momentum exchange rate.

The energy conservation Eqs. (7) and (8) are simply the Fourier transformed fluid continuity and momentum equations, where the internal and kinetic nonlinear transfer terms T_n and T_u are not related to a specific preassumed wave coupling form, and are simply derived from the convective derivatives in the continuity and momentum equations. Therefore the properties of internal and kinetic energy transfer terms are very basic and physical. By expanding the vector identities for a magnetized plasma with $\mathbf{B}=B\hat{z}$, the internal and kinetic energy transfer terms can be rewritten as

$$T_n(\omega) \equiv \left\langle -\mathrm{Re}\left[\sum_{\omega_1} n_\omega^*(\hat{z}\times\nabla_\perp\phi_{\omega-\omega_1}\cdot\nabla_\perp)n_{\omega_1}\right]\right\rangle$$
$$\approx \left\langle \mathrm{Re}\left[\sum_{\substack{\omega_1=+f_{nyq}\\ \omega_1=-f_{nyq}\\ |\omega-\omega_1|\le f_{nyq}}} n_\omega^*\left(\frac{\partial\phi_{\omega-\omega_1}}{\partial y}\frac{\partial n_{\omega_1}}{\partial x} - \frac{\partial\phi_{\omega-\omega_1}}{\partial x}\frac{\partial n_{\omega_1}}{\partial y}\right)\right]\right\rangle, \tag{9}$$

$$T_u(\omega) \equiv \left\langle -\mathrm{Re}\sum_{\omega_1}(\hat{z}\times\nabla_\perp\phi_\omega^*)\cdot[(\hat{z}\times\nabla_\perp\phi_{\omega-\omega_1}\cdot\nabla_\perp)(\hat{z}\times\nabla_\perp\phi_{\omega_1})]\right\rangle$$
$$\approx \left\langle \mathrm{Re}\sum_{\substack{\omega_1=+f_{nyq}\\ \omega_1=-f_{nyq}\\ |\omega-\omega_1|\le f_{nyq}}} \left[\frac{\partial\phi_\omega^*}{\partial x}\left(\frac{\partial\phi_{\omega-\omega_1}}{\partial y}\frac{\partial^2\phi_{\omega_1}}{\partial x^2} - \frac{\partial\phi_{\omega-\omega_1}}{\partial x}\frac{\partial^2\phi_{\omega_1}}{\partial x\,\partial y}\right) + \frac{\partial\phi_\omega^*}{\partial y}\left(\frac{\partial\phi_{\omega-\omega_1}}{\partial y}\frac{\partial^2\phi_{\omega_1}}{\partial x\,\partial y} - \frac{\partial\phi_{\omega-\omega_1}}{\partial x}\frac{\partial^2\phi_{\omega_1}}{\partial y^2}\right)\right]\right\rangle, \tag{10}$$

where x (y) denote the radial (azimuthal or poloidal) directions, respectively.

With energy balance Eqs. (7) and (8), it can be seen that T_n and T_u are actually energy flow rate. If T_n is positive while all other terms in Eq. (7) are constant, then the energy term $|n_\omega|^2$ will grow; if T_n is negative then $|n_\omega|^2$ decreases. Similarly positive T_u renders a growth in $|\nabla\phi_\omega|^2$ while negative T_u renders a decrease in $|\nabla\phi_\omega|^2$. Therefore the bispectral terms T_n and T_u in the energy balance equations not only tell how various three-wave interactions transfer energy into or out of fluctuations with frequency ω, but also can be used to determine the rate and direction of the nonlinear energy transfer.

By splitting the T_n and T_u into parts, more detailed physics can be obtained. For example, if the first part,

$$\mathrm{Re}\left[\frac{1}{M}\sum_{k=1}^{M}\frac{\partial\phi_\omega^*}{\partial x}\frac{\partial\phi_{\omega-\omega_1}}{\partial y}\frac{\partial^2\phi_{\omega_1}}{\partial x^2}\right]_k,$$

of the expanded form of the kinetic energy transfer term is positive (where k denotes the kth ensemble of a total of M available ensembles), it means $|\nabla_\perp\phi_\omega|^2$ is gaining energy because $\partial\phi_{\omega-\omega_1}/\partial y$ and $\partial^2\phi_{\omega_1}/\partial x^2$ interact to give energy to $\partial\phi_\omega/\partial x$. Or physically this means that $u_\theta(\omega)$ gains energy from the radial velocity $u_r(\omega-\omega_1)$ and the azimuthal velocity shear $\partial u_\theta(\omega_1)/\partial r$.

If the Fourier transformed conservation equation [e.g., Eq. (4) or (8)] is to exist for all frequencies, it is necessary that the equation satisfies a slowly varying assumption for all frequencies of interest. Thus if the conservation equation is written as $A(t)=0$ then the Fourier transform $A_\omega(t)$ will exist only if $[1/A_\omega(t)][\partial A_\omega(t)/\partial t]\ll\omega$ for the frequencies of interest. This assumption must be verified from the experimental data.

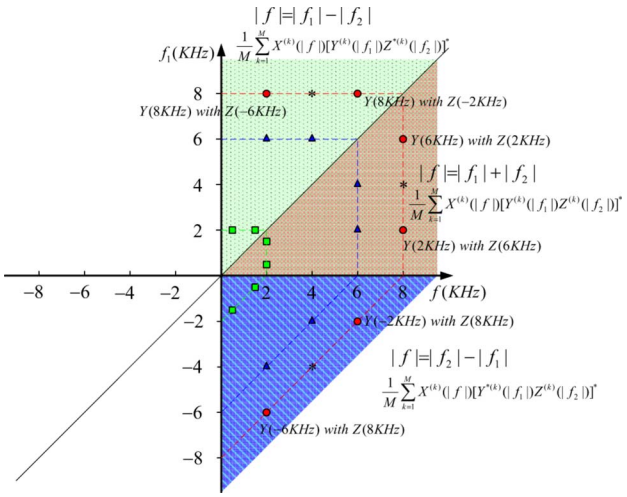

FIG. 1. (Color online) Calculation region for three-field (X, Y, and Z) cross bispectrum and cross bicoherence. The x-axis is for field X and y-axis is for field Y. Gray (red): $f,f_1,f_2>0$, means that the way $Y(f_1)$ and $Z(f_2)$ interact is $|f|=|f_1|+|f_2|$, and the phase relation is $\theta_X(f)=\theta_Y(f_1)+\theta_Z(f_2)$. Light gray (green): $f,f_1>0$ and $f_2<0$, the frequency relation is $|f|=|f_1|-|f_2|$, and the phase relation is $\theta_X(f)=\theta_Y(f_1)-\theta_Z(|f_2|)$. Dark gray (blue): $f,f_2>0$ and $f_1<0$, the frequency relation is $|f|=|f_2|-|f_1|$, and the phase relation is $\theta_X(f)=\theta_Y(f_2)-\theta_Z(|f_1|)$.

The calculation and interpretation of the above T_n and T_u needs a thorough understanding of the three-field cross bispectrum. The autobispectrum introduced by Kim and Powers[11] can be easily generalized to measure the phase coherence among three different fields. The cross bispectrum is defined as

$$\hat{S}_{XYZ}(f_1,f_2) \equiv E[(X(f)Y^*(f_1)Z^*(f_2))]$$
$$= \frac{1}{M}\sum_{k=1}^{M}[X(f)Y^*(f_1)Z^*(f_2)]_k, \tag{11}$$

or writing each signal in terms of an amplitude and phase, it can alternatively be written as

$$\hat{S}_{XYZ}(f_1,f_2) \equiv \frac{1}{M}\sum_{k=1}^{M}[|X(f)Y^*(f_1)Z^*(f_2)|e^{i\delta\theta}]_k, \tag{12}$$

where $\delta\theta\equiv\theta_X(f)-\theta_Y(f_1)-\theta_Z(f_2)$ denotes the phase mismatch for a given ensemble. Clearly if $\delta\theta$ varies randomly across the ensemble average (i.e., if the random phase approximation is satisfied) then $\hat{S}_{XYZ}(f_1,f_2)$ will vanish; alternatively if $\delta\theta$ has a reproducible range of values across the ensemble average, then $\hat{S}_{XYZ}(f_1,f_2)$ will have a finite value and since the cross bispectrum is related to the energy transfer in the Fourier domain, there will be a finite exchange of energy between the involved frequencies in such cases. The calculation region can be greatly reduced because of the symmetry properties of the cross bispectrum and by the fact that often the fluctuation frequencies of interest are much smaller than the Nyquist frequency. Figure 1 shows the typical calculation region for the three-field cross bispectrum

TABLE I. A layout of all possible combinations of three-wave interactions with different frequencies: 8, 6, and 2 kHz.

X	8 kHz	8 kHz	6 kHz	6 kHz	2 kHz	2 kHz
Y	2 kHz	6 kHz	8 kHz	−2 kHz	8 kHz	−6 kHz
Z	6 kHz	2 kHz	−2 kHz	8 kHz	−6 kHz	8 kHz

with light gray (green), gray (red), and dark gray (blue) triangles, where the interested frequencies (assumed $\leq$9.5 KHz) are much smaller than the typical Nyquist frequency. Suppose that three different plasma waves with frequencies, e.g., 8, 6, and 2 kHz, interact with each other. There will be a total of six different permutations for this interaction as shown by Table I, where each column stands for a different physical coupling process since it involves coupling among three fields (X, Y, and Z). For one-field couplings where $X=Y=Z$, i.e., the autobispectrum or autobicoherence, these six different combinations stand for exactly the same physical process.

In Fig. 1, with the x-axis for field X and y-axis for field Y, all six different combinations are indicated accordingly by the red dots. In the region with gray (red) color ($f,f_1,f_2>0$) $Y(f_1)$ and $Z(f_2)$ interact so that $|f|=|f_1|+|f_2|$, and the phase relation is $\theta_X(f)=\theta_Y(f_1)+\theta_Z(f_2)$, e.g., for the dot at ($f=8$ kHz, $f_1=2$ kHz) we can infer that f_2 corresponding to field Z must be 6 kHz, and the phase relation for this coupling must be $\theta_X(8\ \text{kHz})=\theta_Y(2\ \text{kHz})+\theta_Z(6\ \text{kHz})$. In the light gray (green) region, $f,f_1>0$ and $f_2<0$, the frequency relation is $|f|=|f_1|-|f_2|$, and the phase relation is $\theta_X(f)=\theta_Y(f_1)-\theta_Z(|f_2|)$. In the dark gray (blue) region, $f,f_2>0$ and $f_1<0$, the frequency relation is $|f|=|f_2|-|f_1|$, and the phase relation is $\theta_X(f)=\theta_Y(f_2)-\theta_Z(|f_1|)$. Since the frequency selection rule for three-wave coupling is typically written as $f=f_1+f_2$, negative frequencies are used here to correspond to physical processes when two frequencies subtract to generate the third, e.g., f_1 subtract f_2 to generate f.

III. EXPERIMENTAL MEASUREMENT OF MULTIFIELD NONLINEAR ENERGY TRANSFER

In this paper the radial direction is denoted as $\hat{x}$, and the azimuthal or poloidal direction is denoted as $\hat{y}$ direction. To experimentally determine the internal energy transfer term T_n one can measure the density and potential fluctuations, compute their derivatives in the radial and azimuthal directions, Fourier transform those quantities into frequency domain to find n_ω, $\partial n_\omega/\partial x$, $\partial n_\omega/\partial y$ and $\partial\phi_\omega/\partial x$, $\partial\phi_\omega/\partial y$, and finally construct T_n by convolution. For the kinetic energy transfer T_u, plasma potential and its first and second derivatives are needed. The quantities needed to infer both T_n and T_u can be obtained experimentally using the spatial layout of density and potential measurements shown in Fig. 2.

In this figure potential channels are indicated by blue and density channels by red. For a cylindrical plasma, which is typical in linear or toroidal machines, the direction relationships are $\hat{x}\leftrightarrow\hat{r}$ and $\hat{y}\leftrightarrow\hat{\theta}$. Finite difference method can be used to compute all derivatives. For example, the central finite difference approximation can be used to calculate $\partial\phi/\partial x|_{x=x_i}\approx(\phi_{i+1}-\phi_{i-1})/(2\Delta x)$ with a leading error of $(\Delta x)^2$, and $\partial^2\phi/\partial x^2|_{x=x_i}\approx(\phi_{i-1}+\phi_{i+1}-2\phi_i)/(\Delta x)^2$ with a leading error of $(\Delta x)^2$. With additional grid points, a higher accuracy of finite difference can be achieved. In experiments, the choice of Δx should be much less than the size of typical turbulent structures, and at the same time be big enough so that the phase difference among adjacent tips is measurable. In our experiment, the typical turbulent correlation lengths are 0.6–2 cm,[25] the ion sound radius is $\rho_S=(C_s/\Omega_{C_i})\sim 1$ cm, and the spatial separations between tips are 1.5 mm in radial direction and 2.5 mm in azimuthal direction.

Because all the derivatives are computed in a rectangular coordinate for cylindrical plasmas in our experiment, it is required that the plasma scale is much larger than the scale of the measurement array. Alternatively one can layout the grid points on magnetic surfaces and correspondingly uses a cylindrical coordinate to compute all the derivatives. The layout in Fig. 2 is set up such that the center of potential channels is the same as the center of density channels in both azimuthal and radial directions, which makes every calculated derivative centered and thus eliminates the phase shift in both radial and azimuthal directions. If the two 3×3 array are spatially shifted by a displacement vector $\delta\mathbf{x}$ relative to each other, then the phase shift $\mathbf{k}\cdot\delta\mathbf{x}$ incurred from this effect due to the wavenumber $\mathbf{k}$ would need to be accounted for in computing the cross spectral quantities. As long as this shift is small compared to the turbulence scale lengths, then such a correction can in principle be applied. In our experiment, the two 3×3 arrays are shifted by 1.5 mm along the magnetic field line, but the corresponding phase shift is negligible since $k_\parallel \ll k_\perp$ for the fluctuations. Generally the density and potential (or velocity) field can be measured in a variety of ways, such as Langmiur probe, heavy ion beam probe[26] or velocimetry of BES.[27] For the study of plasmas in

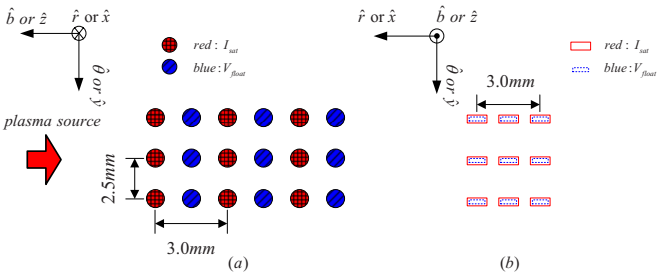

FIG. 2. (Color online) Spatial layout of the measurement grid points. (b) is the side view of (a). All the probe tips are identical, but the V_{float} tips were purposely drawn smaller in (b) in order to distinguish the I_{sat} tips from V_{float} tips. All the derivatives $\partial\phi/\partial x$, $\partial\phi/\partial y$, $\partial^2\phi/\partial x^2$, $\partial^2\phi/\partial y^2$, and $\partial^2\phi/\partial x\partial y$ can be computed using finite difference method from the nine channels of potential [dark gray (blue)]. n, $\partial n/\partial x$, and $\partial n/\partial y$ can be computed from the nine channels of density [gray (red)].

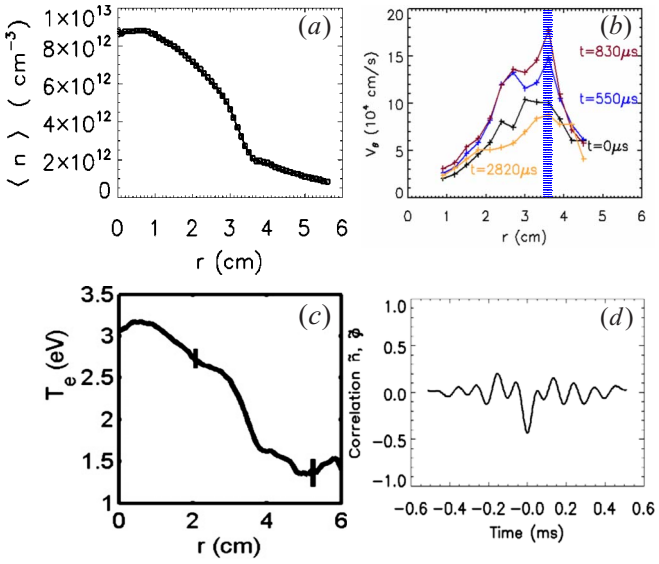

FIG. 3. (Color online) (a) Time-averaged plasma density. (b) Time resolved plasma azimuthal velocity profile calculated from 2D visible light imaging using time delay estimation [Figure reprinted with permission from Ph.D. thesis of Yan Z (Ref. 29).] It is found that the velocity at the shadowed region $r \sim 3.6$ cm develops and decays at the frequency around 250 Hz. (c) Time-averaged electron temperature profile. [Reprinted with permission from G. R. Tynan *et al.*, Phys. Plasmas **11**, 5195 (2004).] (d) Correlation between density and potential fluctuations at shear layer.

linear devices or edge plasmas in tokamaks, a multipoint Langmuir probe array is a good candidate for its excellent spatial resolution, relative easiness to design and construct, and the lower cost compared to other techniques. However, we explicitly note that such nonlinear energy transfer studies are also possible with these other diagnostic approaches provided that the necessary multipoint data can be obtained.

The experiment for nonlinear energy transfer measurement has been carried out on a cylindrical linear plasma device CSDX in the University of California, San Diego. For the experiments reported here the discharges were operated with 1000 Gauss magnetic field and 3.0 mtorr argon filling pressure, the helicon plasma source was operated at 13.56 MHz with a power of 1.5 KW; the resulting plasma had a peak on-axis density $\sim 10^{13}$ cm^{-3} and on-axis electron temperature ~ 3 eV. The plasma source has a diameter of 10 cm, and the vacuum chamber is with a diameter of 20 cm. Further details about the device and characteristics of the plasma and of the transition to a state of weak turbulence can be found elsewhere.[19,28]

A dual 3×3 tip Langmuir array has been built and installed on CSDX, which enables us to simultaneously measure nine channels of plasma density and nine channels of floating potential on an x-y grid, as shown in Fig. 2. Therefore all the quantities needed for constructing the internal and kinetic energy transfer terms can be obtained by this probe array. Although for the purpose of measuring energy transfer only the first derivatives of density are needed, thus four channels of density are enough, the five redundant density channels either can be used to compute the second derivatives or can be setup for other purposes such as triple probe array to measure plasma potential and electron temperature. A general concern could be that the layout of I_{sat} and floating potential tips would introduce a shadowing effect among them, especially between I_{sat} and floating potential tips, and thus could distort the measured bispectra. Experiments have been carried out to compare the obtained kinetic energy transfer coefficients at the conditions with or without I_{sat} bias voltage. No significant differences have been found between these two cases suggesting that any such shadowing effects are small.

IV. EXPERIMENTAL RESULTS

Figure 3 shows the typical profiles of CSDX plasma operated with a magnetic field of 1000 G, an argon fill pressure of 3.0 mtorr, and a rf power input of 1.5 KW. The plasma density profile presented in Fig. 3(a) is measured by the 18-tip probe array. Figure 3(b) shows the plasma azimuthal velocity profile calculated from two-dimensional (2D) visible light imaging using a time delay estimation technique. We find that the azimuthal velocity grows and decays with a frequency of ~ 250 Hz; the radial profiles show that the shearing rate also varies in magnitude at the same frequency.[29] Previous results, which were obtained by ensemble averaging over many such oscillation cycles showed that the resulting time-averaged shear flow is consistent with the measured time-averaged turbulent Reynolds stress and the estimated damping profiles.[1] As we show below, the bispectral calculation shows that both internal and kinetic energy are transferred from drift turbulence to this velocity oscillation. Figure 3(c) is the time-averaged electron temperature profile taken from a previous published paper.[28]

All the potential and density channels were simultaneously sampled at 500 kHz, and the total sampling time was 10 s. So for each channel, a total of 5×10^6 sampling points has been acquired, which were then divided into one to sev-

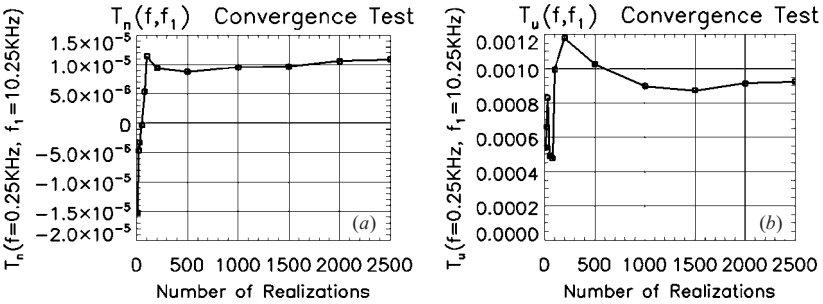

FIG. 4. Convergence test for the bispectral calculation for the internal and kinetic energy transfer terms $T_n(f,f_1)$ and $T_u(f,f_1)$ at the frequencies $f=0.25$ kHz and $f_1=10.25$ kHz. (a) is for $T_n(f=0.25$ kHz, $f_1=10.25$ kHz) and (b) is for $T_u(f=0.25$ kHz, $f_1=10.25$ kHz).

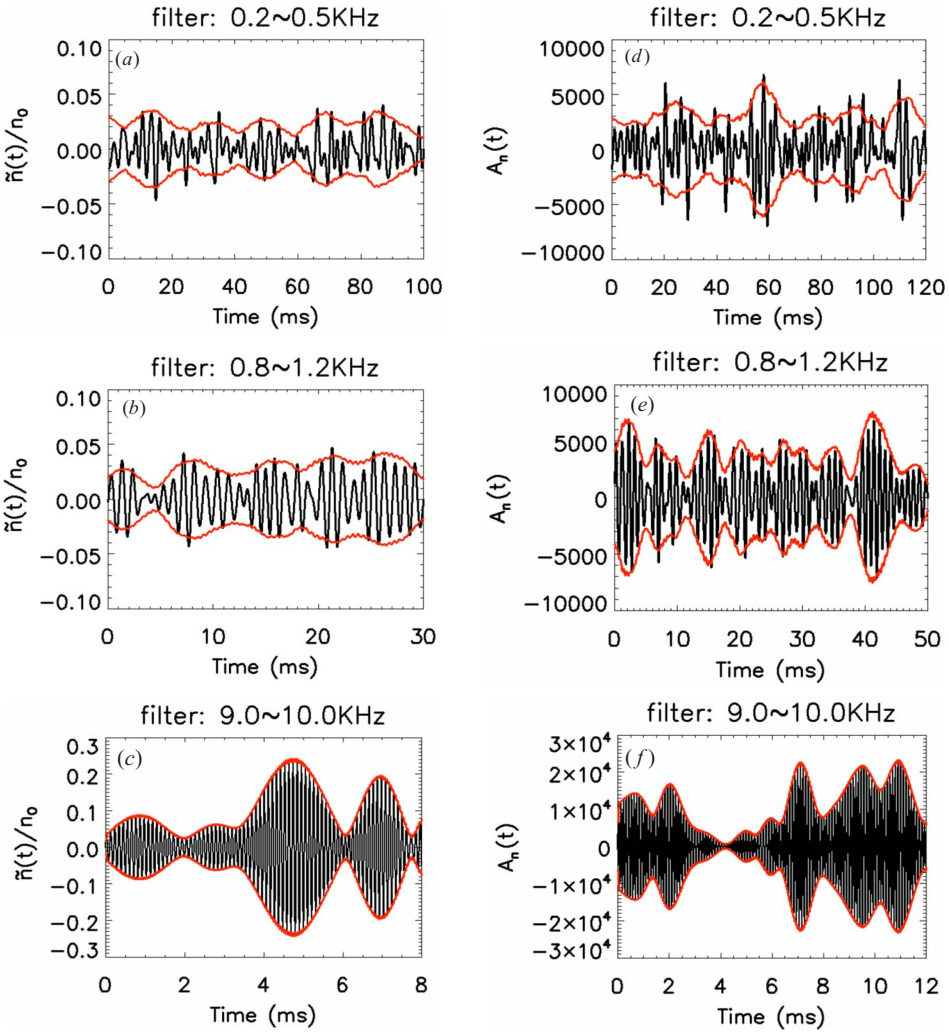

FIG. 5. (Color online) (a) 0.2–0.5 kHz bandpass-filtered density fluctuation $\tilde{n}(t)$ plotted as a function of time. The envelope shows a period of 15–20 ms, indicating a slowly variation of the spectra at 0.2–0.5 kHz. (b) 0.8–1.2 kHz bandpass-filtered density fluctuation. The envelope has a period of 6–9 ms. (c) 9.0–10.0 kHz filtered density fluctuation with a enveloped period of 2–4 ms. (d) 0.2–0.5 kHz bandpass-filtered total derivative of density fluctuation $A(t) \equiv [(\partial/\partial t) + \vec{u} \cdot \nabla] n(t)$ plotted as a function of time. The envelope shows a period of 15–20 ms, indicating a slowly variation of the spectra at 0.2–0.5 kHz. (e) 0.8–1.2 kHz bandpass-filtered total derivative of density fluctuation. The envelope has a period of 8–10 ms. (f) 9.0–10.0 kHz filtered total derivative of density fluctuation with a enveloped period of 3–4 ms.

eral thousand independent realizations to produce statistically converged bispectra by ensemble averaging. Figure 4 shows the convergence test for the bispectral calculation of the internal and kinetic energy transfer terms $T_n(f,f_1)$ and $T_u(f,f_1)$ at the frequencies $f=0.25$ kHz and $f_1=10.25$ kHz. There we can see that both the internal and kinetic bispectra reasonably converge when at least ~1000 realizations are used. As is shown below, the existence of very slowly varying nonlinearly driven fluctuations such as zonal flows imposed a physics requirement for high frequency resolution. This requirement, combined with the large number of ensembles required for convergence implies the requirement for long time series (with $\sim 10^7$ samples per channel) and highly stationary experimental conditions. A similar number of realizations are required to converge at other combinations of f and f_1.

Before examining the nonlinear turbulence energy transfer processes of interest, it is important to determine if the ansatz $[1/|n_\omega(\underline{x},t)|][\partial|n_\omega(\underline{x},t)|/\partial t] \ll \omega$ is satisfied. To determine this, the experimentally measured density was first normalized by its time-averaged value, and then bandpass filtered for several representative frequency ranges. The relevant frequency ranges are chosen based upon previously published spectral results[19] and plotted as a function of time in Figs. 5(a)–5(c). Figure 5(a) corresponds to the bandpass filtered over a range 0.2–0.5 kHz, in which the envelope of density fluctuations varies with a period of 15–20 ms (50–37 Hz), a factor of 6 slower than the corresponding phase change frequency approximated by the center value of the filter. Figure 5(b) is density fluctuation filtered by 0.8–1.2 kHz, where the envelope shows a period of 6–9 ms (110–170 Hz), i.e., a factor of ~10× slower variation than the fluctuation frequency. Figure 5(c) is the density fluctuation filtered by 9.0–10.0 kHz, and the envelope is with a period of 2.0–2.3 ms (430–500 Hz), which again is a factor of ~10–20× longer than the fluctuation period under consideration. Thus from Figs. 5(a)–5(c) we can tell that in our linear device the amplitude of density fluctuations varies by factors of ~5–20× slower than the corresponding phase changes. By following the same process, it has been verified that this is also true for $\nabla_\perp \phi$. Figures 5(d) through 5(f) show similar results calculated for the left hand side of Eq. (2) from measured data. We therefore conclude from this study that the slowly varying assumption is reasonably well satisfied by the experimental data.

The internal and kinetic energy transfer functions derived in this manner are shown in Fig. 6, which was obtained when the probe was centered on the shear layer located at $r=3.6$ cm, with magnetic field of 1000 G, rf power of 1.5 kW, and pressure of 3.0 mtorr. These conditions are the

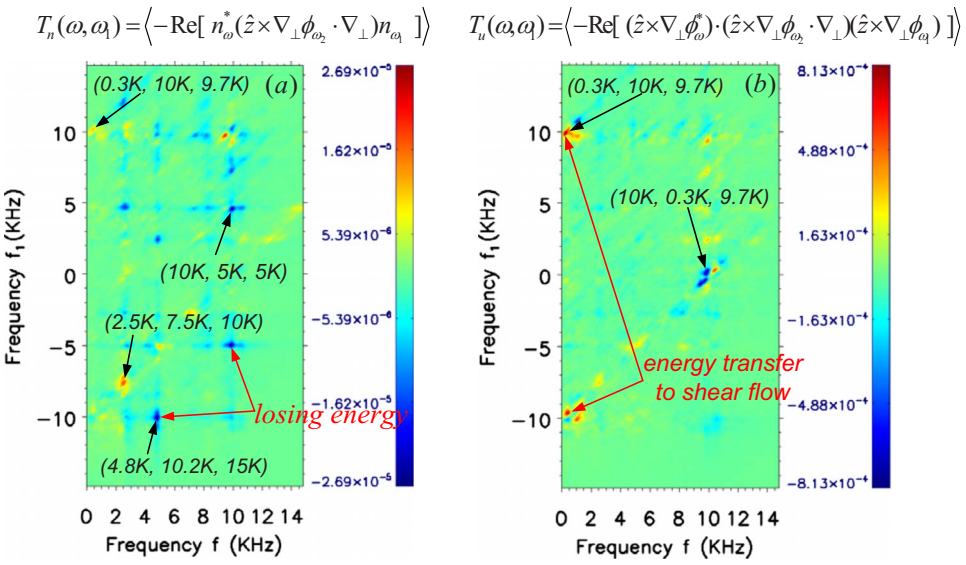

FIG. 6. (Color online) Measurement is taken at $r=3.6$ cm, magnetic field of 1000 G, rf power of 1.5 kW, and pressure of 3.0 mtorr. (a) Bispectral internal energy transfer $T_n(\omega,\omega_1)$ [in both (a) and (b) the x-axis corresponds to ω and y-axis corresponds to ω_1 in Eqs. (7) and (8), and notation $\omega_2=\omega-\omega_1$]. (b) Bispectral kinetic energy transfer $T_u(\omega,\omega_1)$.

same as those used to study the origin of the shear layer in previous work.[1,5] In computing the bispectra in Fig. 6, for each channel a total of 5×10^6 samples were divided into 1200 ensembles, with 4096 samples in each ensemble. Since a sampling frequency of 500 kHz was used when acquiring the data, the frequency resolution in Fig. 6 is about 120 Hz. Figure 6(a) shows the internal energy transfer $T_n(\omega,\omega_1)$, and Fig. 6(b) shows the kinetic energy transfer coefficient $T_u(\omega,\omega_1)$.

From the energy balance Eqs. (7) and (8), we know that positive (negative) internal or kinetic energy transfer means that fluctuations at frequency ω gain (lose) energy through the wave-wave interaction with ω_1 and $\omega-\omega_1$. In both plots the x-axis is ω and y-axis is ω_1. Several prominent three-wave coupling triplets are indicated in these two figures, such as the triplet (10 K, 5 K, 5 kHz) in Fig. 6(a). The negative value for $T_n(\omega,\omega_1)$ at ($\omega=10$ kHz, $\omega_1=5$ kHz) means that density fluctuation n at 10 kHz loses energy to either $\nabla_\perp\phi$ at 5 kHz or $\nabla_\perp n$ at 5 kHz ($\omega-\omega_1=5$ kHz). There is an uncertainty of which frequency is receiving energy because we can only tell from the energy conservation Eq. (7) that the frequency ω is gaining or losing energy, but it is not possible to determine into which wave the energy is moving. Similarly in Fig. 6(b) the positive value for $T_u(\omega,\omega_1)$ at ($\omega=0.3$ kHz, $\omega_1=10$ kHz) means that the velocity $(\hat{z}\times\nabla_\perp\phi/B)$ at 9.7 kHz interacts with the vorticity $\nabla_\perp^2\phi$ at 10 kHz to transfer energy to the velocity fluctuation occurring at 0.3 kHz. The frequency and wave number resolved two-point estimated spectrum has been measured on CSDX,[1] which shows that small scale drift turbulence is typically with a k_θ bigger than 1 cm^{-1} and with a frequency of several kilohertz to 20 kHz, while large-scale azimuthal flow has both the k_θ and frequency close to zero. By using this measured local spectra, we can conclude that the positive value for $T_u(\omega,\omega_1)$ at ($\omega=0.3$ kHz, $\omega_1=10$ kHz) in Fig. 6(b) is a clear sign of energy transfer from a turbulent flow to a large-scale shear flow since we have found that this 0.3 kHz velocity fluctuation is associated with the slow evolution of the sheared zonal flow as summarized above and shown in detail elsewhere.[29] In Fig. 6(b) the negative value for T_u at ($\omega=10$ kHz, $\omega_1=0.3$ kHz) means the velocity at 10 kHz loses energy through three-wave coupling with $\nabla_\perp^2\phi$ at 0.3 kHz and the velocity at 9.7 kHz. If we expand T_u into four different parts and calculate them separately from experimental data, we will find that there is one part,

$$\mathrm{Re}\left\{\frac{1}{M}\sum_{k=1}^{M}\left[\frac{\partial\phi_\omega^*}{\partial x}\frac{\partial\phi_{\omega-\omega_1}}{\partial y}\frac{\partial^2\phi_{\omega_1}}{\partial x^2}\right]_k\right\},$$

that dominates others. This means that the nonlinear kinetic energy transfer to azimuthal shear flow is mostly due to the radial flux of vorticity (due to the fact that in the experimental data $\partial^2\phi/\partial x^2$ dominates $\partial^2\phi/\partial y^2$ and $\partial^2\phi/\partial x\partial y$ in the expansion form of $\nabla_\perp^2\phi$). Or it can be interpreted that azimuthal velocity shear couples with radial velocity to transfer energy to shear flow. The internal energy transfer also has a similar feature. These relevant arguments and physical interpretation will be covered in a separate paper.

V. SUMMARY AND DISCUSSIONS

In this paper, a method for studying the nonlinear energy transfer with a two-field (density and potential) model, including both theoretical derivation and experimental setup, is proposed and explained. Experimental results measured at the shear layer give a clear picture of wave coupling and energy transfer. This is the first time that nonlinear energy transfer is experimentally studied using a two-field model in frequency domain.

Calculating bispectrum (essentially a convolution) is slow and computationally expensive. Instead of doing convolutions in frequency domain, an alternate way to calculate the nonlinear energy transfer coefficients is to first construct an effective time series in real time domain using time series of density and potential, then take the Fourier transform of the constructed time series to get energy transfer coefficients. This approach is much faster than directly calculating bispectra in frequency domain. For example, the internal energy transfer coefficient can be formulated as

$$T_n \equiv \left\langle -\mathrm{Re}\sum_{\omega_1} n_\omega^*(\hat{z}\times\nabla_\perp\phi_{\omega-\omega_1}\cdot\nabla_\perp)n_{\omega_1}\right\rangle$$
$$\approx \left\langle \mathrm{Re}\sum_{\substack{\omega_1=-f_{nyq}\\ |\omega-\omega_1|\le f_{nyq}}}^{\omega_1=+f_{nyq}} n_\omega^*\left(\frac{\partial\phi_{\omega-\omega_1}}{\partial y}\frac{\partial n_{\omega_1}}{\partial x}-\frac{\partial\phi_{\omega-\omega_1}}{\partial x}\frac{\partial n_{\omega_1}}{\partial y}\right)\right\rangle. \quad (13)$$

However it can also be reformulated as

$$T_n \equiv \left\langle -\mathrm{Re}\sum_{\substack{\omega_1,\omega_2\\ \omega=\omega_1+\omega_2}} n_\omega^*(\hat{z}\times\nabla_\perp\phi_{\omega_1}\cdot\nabla_\perp)n_{\omega_2}\right\rangle$$
$$= \left\langle \mathrm{Re}\left\{[\mathrm{FFT}(n)]^*\mathrm{FFT}\left[\frac{\partial\phi}{\partial y}\frac{\partial n}{\partial x}-\frac{\partial\phi}{\partial x}\frac{\partial n}{\partial y}\right]\right\}\right\rangle. \quad (14)$$

According to Eq. (14), one can first construct a time series $[(\partial\phi/\partial y)(\partial n/\partial x)]-[(\partial\phi/\partial x)(\partial n/\partial y)]$, then take the cross power of density n and this effective time series. Note that this approach can only produce the coefficients summed over ω_1. When one desires to determine the interacting triplets, then the results contained in Figs. 6(a) and 6(b) are needed and the method computing convolution should be used. Due to finite signal sampling frequency of real data acquisition systems, these two methods may produce slightly different curves [difference comes from the fact that fast Fourier transform (FFT) of a finite time series is defined from circular convolution instead of a linear convolution]. However, when the sampling frequency is sufficiently high, the difference is negligible. We plan to discuss this approach and comparing it to the cross-bispectral technique in a separate paper.

The method proposed in this paper is completely in frequency domain. The disadvantage of this approach is that it is not formulated in wavenumber space which may make comparison with analytic theory and simulation more difficult (although in principle simulations can calculate these quantities in frequency space exactly, provided that they are run for enough time and that any possible frame transformation between laboratory and plasma center of mass frame due to bulk rotation is accounted for). One way to overcome this difficulty could be combining these results with a measured dispersion relation to relate frequencies to azimuthal wave numbers. Also note that in this experiment, floating potential instead of plasma potential is used to calculate electric field and the fluid velocity. This approach has essentially neglected the effect introduced by electron temperature fluctuations. One interesting future work could be including density, potential, and temperature fluctuations to study the quadratic nonlinearity in a three-field model via a straightforward extension of this approach to such a system.

ACKNOWLEDGMENTS

This research was supported by the U.S. Department of Energy (DOE) through Grant No. DE-FG02-OER54871.

[1] G. R. Tynan, C. Holland, J. H. Yu, A. James, D. Nishijima, M. Shimada, and N. Taheri, Plasma Phys. Controlled Fusion **48**, S51 (2006).
[2] P. H. Diamond, S. I. Itoh, K. Itoh, and T. S. Hahm, Plasma Phys. Controlled Fusion **47**, R35 (2005).
[3] F. W. Perkins, C. W. Barnes, D. W. Johnson, S. D. Scott, M. C. Zarnstorff, M. G. Bell, R. E. Bell, C. E. Bush, B. Grek, K. W. Hill, D. K. Mansfield, H. Park, A. T. Ramsey, J. Schivell, B. C. Stratton, and E. Synakowski, Phys. Fluids B **5**, 477 (1993).
[4] J. P. Christiansen, P. M. Stubberfield, J. G. Cordey, C. Gormezano, C. W. Gowers, J. O'rourke, D. Stork, A. Taroni, and C. D. Challis, Nucl. Fusion **33**, 863 (1993).
[5] C. Holland, J. H. Yu, A. James, D. Nishijima, M. Shimada, N. Taheri, and G. R. Tynan, Phys. Rev. Lett. **96**, 195002 (2006).
[6] G. R. Tynan, R. A. Moyer, and M. J. Burin, Phys. Plasmas **8**, 2691 (2001).
[7] A. Hasegawa and C. G. Maclennan, Phys. Fluids **22**, 2122 (1979).
[8] C. P. Ritz and E. J. Powers, Physica D **20**, 320 (1986).
[9] J. S. Kim, R. J. Fonck, R. D. Durst, E. Fernandez, P. W. Terry, S. F. Paul, and M. C. Zarnstorff, Phys. Rev. Lett. **79**, 841 (1997).
[10] Y. C. Kim, J. M. Beall, E. J. Powers, and R. W. Miksad, Phys. Fluids **23**, 258 (1980).
[11] Y. C. Kim and E. J. Powers, IEEE Trans. Plasma Sci. **7**, 120 (1979).
[12] C. W. Van Atta and J. C. Wyngaard, J. Fluid Mech. **72**, 673 (1975).
[13] T. T. Yeh and C. W. Van Atta, J. Fluid Mech. **58**, 233 (1973).
[14] C. W. Van Atta and W. Y. Chen, J. Fluid Mech. **38**, 743 (1969).
[15] C. P. Ritz, E. J. Powers, and R. D. Bengtson, Phys. Fluids B **1**, 153 (1989).
[16] J. S. Kim, R. D. Durst, R. J. Fonck, E. Fernandez, A. Ware, and P. W. Terry, Phys. Plasmas **3**, 3998 (1996).
[17] M. D. Millionshchikov, Dokl. Akad. Nauk SSSR **32**, 611 (1941).
[18] G. A. Hallock and A. J. Wootton, Phys. Rev. Lett. **59**, 1301 (1987).
[19] M. J. Burin, G. R. Tynan, G. Y. Antar, N. A. Crocker, and C. Holland, Phys. Plasmas **12**, 052320 (2005).
[20] S. J. Camargo, D. Biskamp, and B. D. Scott, Phys. Plasmas **2**, 48 (1995).
[21] P. Manz, M. Ramisch, U. Stroth, V. Naulin, and B. D. Scott, Plasma Phys. Controlled Fusion **50**, 035008 (2008).
[22] C. Holland, G. R. Tynan, R. J. Fonck, G. R. Mckee, J. Candy, and R. E. Waltz, Phys. Plasmas **14**, 056112 (2007).
[23] G. R. Tynan, P. H. Diamond, O. Gurcan, C. Holland, S. H. Muller, M. Xu, Z. Yan, J. Yu, P. Manz, M. Ramisch, U. Stroth, Y. Nagashima, S. I. Itoh, M. Yagi, S. Inagaki, A. Fujisawa, N. Kasuya, K. Itoh, T. Windisch, O. Grulke, and T. Klinger, 22nd IAEA Fusion Energy Conference, Geneva, Switzerland, 2008, Paper No. IAEA-CN-165/EX/P5-40.
[24] A. Hasegawa and M. Wakatani, Phys. Rev. Lett. **50**, 682 (1983).
[25] Z. Yan, J. H. Yu, C. Holland, M. Xu, S. H. Muller, and G. R. Tynan, Phys. Plasmas **15**, 092309 (2008).
[26] P. M. Schoch, A. Carnevali, K. A. Conner, T. P. Crowley, J. C. Forster, R. L. Hickok, J. F. Lewis, J. G. Schatz, Jr., and G. A. Hallock, Rev. Sci. Instrum. **59**, 1646 (1988).
[27] G. R. Mckee, R. J. Fonck, D. K. Gupta, D. J. Schlossberg, and M. W. Shafer, Rev. Sci. Instrum. **75**, 3490 (2004).
[28] G. R. Tynan, M. J. Burin, C. Holland, G. Antar, and N. Crocker, Phys. Plasmas **11**, 5195 (2004).
[29] Z. Yan, "Turbulent-driven shear slow and self-regulating drift wave turbulence in a cylindrical plasma device," Ph.D. thesis, University of California, 2008.